Heliyon 9 (2023) e22865

Contents lists available at ScienceDirect

Heliyon

journal homepage: www.cell.com/heliyon

Research article

Circular rotation of different structures on natural convection of nanofluid-mobilized circular cylinder cavity saturated with a heterogeneous porous medium

Abdelraheem M. Aly [a,*], Zehba Raizah [a], Ali J. Chamkha [b]

[a] Department of Mathematics, College of Science, King Khalid University, P.O. Box 9004, 61413, Abha, Saudi Arabia
[b] Faculty of Engineering, Kuwait College of Science and Technology, Doha District, Kuwait

ARTICLE INFO

Keywords:
The ISPH method
Porous media
Heterogeneous porous media
Natural convection
Al_2O_3 nanofluid
Circular cylinder
Embedded structures

ABSTRACT

The incompressible smoothed particle hydrodynamics (ISPH) method is utilized for studying the circular rotations of three different structures, circular cylinder, rectangle and triangle centered in a circular cylinder cavity occupied by Al_2O_3 nanofluid. The novelty of this work is appearing in simulating the circular rotations of different solid structures on natural convection of a nanofluid-occupied a circular cylinder. The circular cylinder cavity is suspended by heterogeneous/homogeneous porous media. The embedded structures are taken as a circular cylinder, rectangle and triangle with equal areas. The first thermal condition considers the whole structure is heated, the second thermal condition considers the half of the structure is heated and the other is cooled and the third thermal condition considers the quarter of the structure is heated and the others are cooled. The outer boundary of cylinder cavity is cooled. Due to the small angular velocity $\omega = 3.15$ (low rotational speeds), then the natural convection case will be considered only. The results are representing the temperature, velocity fields. The simulations revealed that the presence of the inner hot/cold structures affects on the velocity distributions and temperature field inside a circular cylinder cavity. The triangle shape has introduced the highest temperature distributions and maximum values of the velocity fields compare to other shapes inside a circular cylinder cavity. The homogeneous porous level reduces the maximum values of velocity field by 25% compared to the heterogeneous porous level.

1. Introduction

Recently, the heat transfer by convection from a cylinder rotating in its container (cavity) is one of the topics of important problems in fluid dynamics due to its enormous applications such as heat exchange of the rotating tube, rotating hubs, fuel rods of nuclear reactor, punching of oil wells, and steel suspension bridge cables. The outer enclosures are applied for minimizing the heat transport from the cylinder in case of rotation. Various experimental and numerical attempts have been presented to simulate the convective flows in the cavities with and without rotating blocks. Hayase et al. [1] investigated the effects of coaxial cylinders embedded inside cavities on mixed convective heat transfer. Fu et al. [2] presented the influence of a circular cylinder rotating near the hot wall of a cavity. They summarized that the natural convective heat transfer can be enhanced by the cylinder rotation's

* Corresponding author.
E-mail address: ababdallah@kku.edu.sa (A.M. Aly).

https://doi.org/10.1016/j.heliyon.2023.e22865
Received 8 January 2023; Received in revised form 31 August 2023; Accepted 21 November 2023

Available online 27 November 2023

Nomenclature

C_p	heat capacity
K_B	Boltzmann's coefficient
Da	Darcy parameter
Pr	Prandtl number
U, V	velocity components
P	dimensionless pressure
k	thermal conductivity
Ra	Rayleigh number
X, Y	Cartesian coordinates
b_x, b_y	base and height of an embedded triangle
W	kernel function
K_0	permeability
u_B	Brownian velocity
$\overline{Nu}$	average Nusselt number
R	radius of a circular cavity
r_c	radius of an embedded cylinder
L_x, L_y	length and width of an embedded rectangle

Greek symbols

μ	dynamic viscosity
η_1	change rate of $\ln(K)$ in X
η_2	change rate of $\ln(K)$ in Y
ζ	thermal conductivity
ρ	density
θ	dimensionless temperature
ϕ	solid volume fraction
τ	dimensionless time
ε	porosity

Subscripts

f	fluid
nf	Nanofluid
p	porous medium
h	hot
c	cold

direction. Oztop et al. [3] have analyzed the effects of a circular body on the combined heat transfer inside a lid-driven square cavity. The readers can find in the references [4–11], different studies of the effects of convection heat transfer due to the rotating circular cylinders. Hussain and Hussein [12] carried out the convection heat transfer of a rotating circular cylinder inside a square enclosure. They found that the location of the rotating cylinder has a good effect on convection heat transfer. In another study in three dimensional, Kareem and Gao [13] investigated the effects of a rotating circular cylinder on the combined convection heat transfer of a 3D blocked cavity. Alsabery et al. [14] carried out a numerical analysis for a solid rotating cylinder inside a wavy porous cavity to illustrate the convective heat transfer.

Ku et al. [15] studied numerically the effect of two small circular cylinders on the accumulation of particles in five different patterns using the flooded boundary method and the discrete element method. Aly [16] presented the effects of the presence of two circular cylinders inside a cavity saturated with a porous medium. Kolsi et al. [17] studied the effects of double-rotating of cylinders on the conductive cooling panel. They considered the influences of cylinder rotational velocities on the cooling operation. Ouri et al. [18] examined the phase change process and convection flow of hybrid nanofluid inside an L-shaped vented cavity containing a rotating cylinder. Selimefendigil et al. [19] analyzed the convective cooling of double-rotating cylinders within a porous medium by adopting hybrid nano-jets. Al-Kouz et al. [20] studied numerically the entropy production and mixed convection in a 3D cavity filled with a phase change material (PCM) and incorporating a rotating cylinder.

In the fluid flows, when both thermal conductivity and permeability are varied, then the porous medium becomes a heterogeneous porous medium. Scientists and researchers give their interest to the thermal convection inside cavities saturated by heterogeneous porous media. The porous environments can be applied in wide branches of engineering. [21–25]. The problems of studying the flow of nanofluids inside different shapes of cavities require specialized discretization techniques and lower computational costs. One of the famous techniques is mesh free methods. The most effective method was the SPH method and many researchers have been used this method for simulating impact flows and fluid-structure interactions [26–32] and fluid flows through porous structures [33–39]. In this simulation, we focus on applying the ISPH method for studying the circular rotations of three different structures, circular cylinder, rectangle and triangle embedded in a circular cylinder cavity filled with a heterogeneous/homogeneous porous media. The circular cavity was filled with $Al_2O_3-H_2O$ nanofluid. The main finding of the performed simulations that the triangle shapes gives the highest temperature distributions and maximum of the velocity field inside a circular cylinder cavity. Moreover, the installation of the inner structures with circular rotations varies the characteristic of the heat and fluid flow inside a circular cavity. This problem can be extended for several industrial applications like rotating-tube heat exchanges and nuclear reactor.

2. Mathematical analysis

This section characterizes the physical model and controlling equations for coupling fluid-structure interactions during natural convection flow. Fig. 1 presents the elementary physical model for embedded three structure, (a) circular cylinder, (b) rectangle, and (c) triangle inside a circular cylinder cavity with their particles models. The structures have been taken with equal areas and their positions were settled in the center of cylinder cavity. The radius of a circular cavity is $R = 0.5$ and its outer boundary is kept at a cold temperature T_c . The embedded structure carries three different thermal conditions including all hot structure, half hot/cold structure and quarter hot and others cold of structure. The structures are circularly rotated around the center in anti-clockwise direction. The radius of the embedded cylinder is $r_c = 0.2$, the length and width of the rectangle are $L_x = 0.4$ and $L_y = 0.3$, respectively. The base and height of the triangle are $b_x = 0.4$ and $b_y = 0.6$.

Table 1
Thermophysical properties of the Al_2O_3 and base fluid (H_2O) at $T = 310$ K [40–42].

Material	$\rho\left(Kgm^{-3}\right)$	$Cp(J/kgK)$	$\beta\times10^{-5}K^{-1}$	$d(nm)$	$K(W/mK)$
H_2O	993	4178	36.2	0.385	0.628
Al_2O_3	3970	765	0.85	33	40

From Fig. 1, the annulus between the embedded structure and outer circular boundary is saturated by a heterogeneous/homogeneous porous medium with a function $\zeta(X,Y)$ and a porosity ε .

The assumptions of the current problem are:

- The structures are modeled by the ISPH method and their motions were circularly rotated around their center.
- One phase model is used for the nanofluid and Darcy model is used for porous media.
- Boussinesq estimation is applied for the density changes.
- Table 1 illustrates the thermo-physical features of Al_2O_3 and H_2O .

The Lagrangian description of the unsteady laminar natural convection flow of a nanofluid according to [41–43] is introduced in following Eqs. (1), (2), (3), (4):

$$\frac{\partial V}{\partial Y} = -\frac{\partial U}{\partial X}, \tag{1}$$

$$\frac{\rho_{nf}}{\varepsilon\rho_f}\frac{dU}{d\tau} + \frac{\rho_{nf}}{\rho_f}\frac{\partial P}{\partial X} + \frac{Pr\mu_{eff}}{\mu_{nf}K^*(X,Y)Da}U = \frac{1}{\varepsilon}\frac{\partial}{\partial X}\left(Pr\frac{\mu_{nf}}{\mu_f}\frac{\partial U}{\partial X}\right) + \frac{1}{\varepsilon}\frac{\partial}{\partial Y}\left(Pr\frac{\mu_{nf}}{\mu_f}\frac{\partial U}{\partial Y}\right) \tag{2}$$

$$\frac{\rho_{nf}}{\varepsilon\rho_f}\frac{dV}{d\tau} + \frac{\rho_{nf}}{\rho_f}\frac{\partial P}{\partial X} + \frac{Pr\mu_{eff}}{\mu_{nf}K^*(X,Y)Da}V = \frac{(\rho\beta)_{nf}}{(\rho\beta)_f}PrRa\theta + \frac{1}{\varepsilon}\frac{\partial}{\partial X}\left(Pr\frac{\mu_{nf}}{\mu_f}\frac{\partial V}{\partial X}\right) + \frac{1}{\varepsilon}\frac{\partial}{\partial Y}\left(Pr\frac{\mu_{nf}}{\mu_f}\frac{\partial V}{\partial Y}\right) \tag{3}$$

$$\frac{\left(\rho c_p\right)_{nf}}{\left(\rho c_p\right)_f}\gamma\frac{d\theta}{d\tau} = \left(\frac{\partial}{\partial X}\left(\zeta(X,Y)\frac{\partial\theta}{\partial X}\right) + \frac{\partial}{\partial Y}\left(\zeta(X,Y)\frac{\partial\theta}{\partial Y}\right)\right) \tag{4}$$

$$K^*(X,Y) = e^{\eta_1 X+\eta_2 Y} \tag{5}$$

$$\zeta(X,Y) = \varepsilon\frac{k_{nf}}{k_f} + (1-\varepsilon)e^{\eta_1 X+\eta_2 Y} \tag{6}$$

$$\gamma = \frac{\varepsilon\left(\rho c_p\right)_{nf} + (1-\varepsilon)\left(\rho c_p\right)_p}{\left(\rho c_p\right)_{nf}} \tag{7}$$

In this study, two levels of porous media including homogeneous porous medium ($\eta_1 = 0$ and $\eta_2 = 0$) and heterogeneous porous medium ($\eta_1 = 0.5$ and $\eta_2 = 0.5$) in Eqs. (5), (6) were considered. Density is ρ , kinematic viscosity is μ . Pressure is P and ε is the porosity. Da is the Darcy parameter, Pr is the Prandtl number, and H is a porous layer height. The parameter γ in Eq. (7) denotes the heat capacity ratio in porous media.

The thermo-physical properties of Al_2O_3- H_2O nanofluid, [44], are introduced in Eqs. (8), (9), (10), (11), (12), (13):

$$\rho_{nf} = \phi\rho_p + (1-\phi)\rho_f, \tag{8}$$

$$\alpha_{nf} = k_{nf}\left(\left(\rho c_p\right)_{nf}\right)^{-1}, \tag{9}$$

$$\left(\rho c_p\right)_{nf} = \phi\left(\rho c_p\right)_p + (1-\phi)\left(\rho c_p\right)_f \tag{10}$$

$$(\rho\beta)_{nf} = \phi(\rho\beta)_p + (1-\phi)(\rho\beta)_f, \tag{11}$$

$$\mu_{nf} = \mu_f\Big/\left(1 - 34.87\left(\frac{d_p}{d_f}\right)^{-0.3}\varphi^{1.03}\right), \tag{12}$$

$$k_{nf} = \left(4.4\left(Re_B\right)^{0.4}Pr^{0.66}\left(\frac{T}{T_{rf}}\right)^{10}\left(\frac{k_p}{k_f}\right)^{0.03}\varphi^{0.66}+1\right)k_f, \tag{13}$$

$$Re_B = \frac{\rho_f u_B d_p}{\mu_f}, \tag{14}$$

$$u_B = \frac{2K_BT}{\left(\pi\mu_f d_p^2\right)}, \tag{15}$$

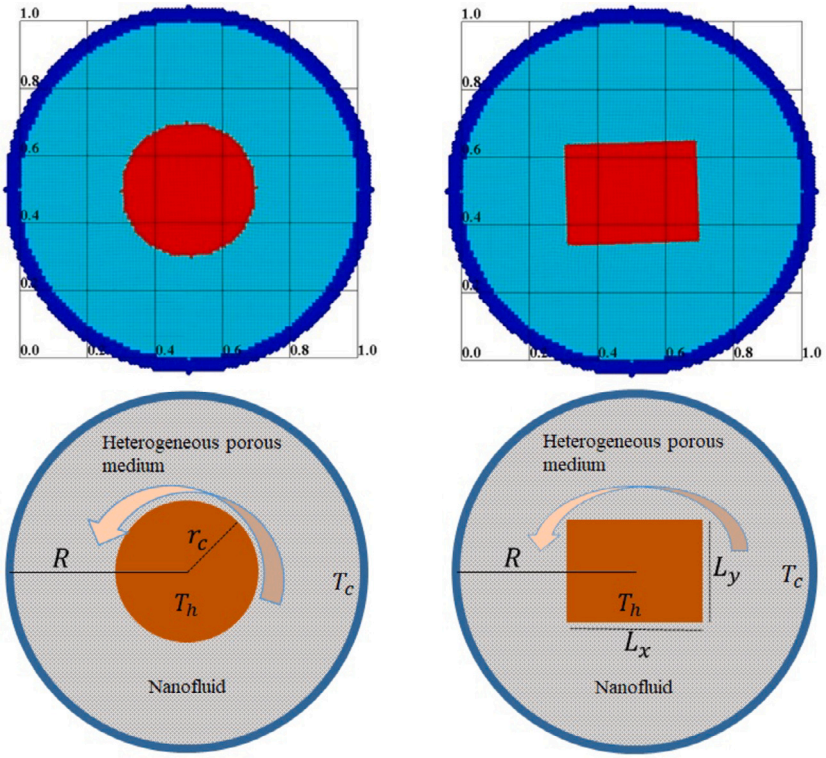

(a) Circular cylinder (b) Rectangle

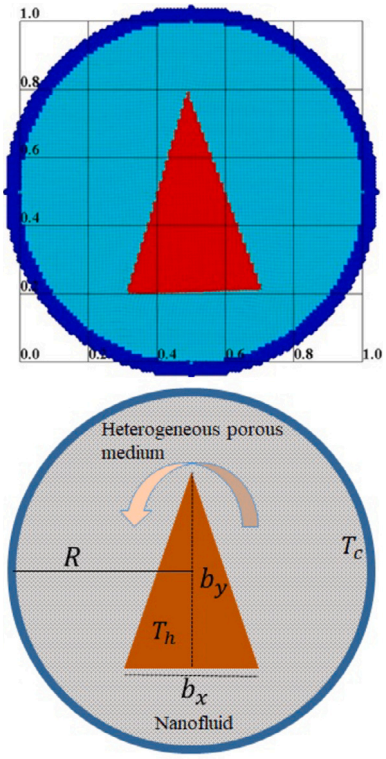

(c) Triangle

Fig. 1. Initial physical model for (a) embedded circular cylinder, (b) embedded rectangle and (c) embedded triangle inside a circular cylinder cavity with their particles models.

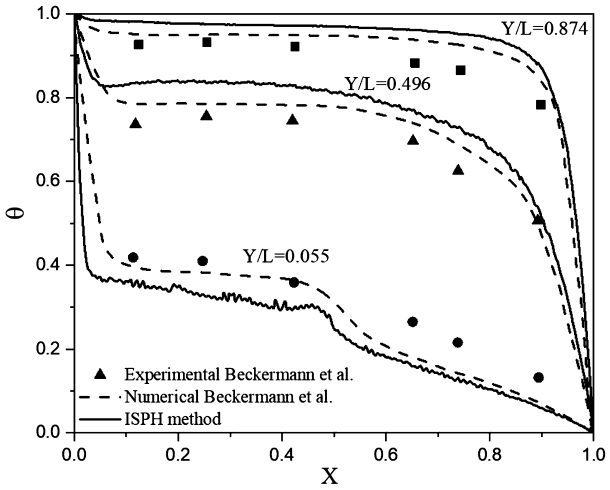

Fig. 2. The temperature profiles in a partial porous cavity from the ISPH method and experimental/numerical results of Beckermann et al. [45].

where, T_{rf} is a water freezing point. In Eqs. (14), (15), $K_B = 1.380648\times10^{-23} J/K$ is Boltzmann's coefficient and u_B is Brownian velocity. The mean Nusselt number:

$$\overline{Nu} = -\frac{\zeta(X,Y)}{S_c}\int_0^{S_c}\frac{\partial\theta}{\partial \mathbf{n}}dY. \tag{16}$$

In Eq. (16), S_c is the length of the outer boundary for a circular cylinder cavity.

3. ISPH method

The solving steps are as follows: predictor velocities (Eqs. (17), (18)), solving pressure Poisson equation (PPE) (Eq. (19)), and corrected velocities (Eqs. (20), (21)). The thermal energy equation is updated in Eq. (22). The particles positioned are updated at each time step in Eqs. (23), (24). Finally, the shifting technique is adopted in this work to adjust the particles positions (Eq. (25)).

$$\frac{(U^*-U^n)}{\varepsilon}\frac{\rho_{nf}}{\rho_f} = \Delta\tau\left(\frac{1}{\varepsilon}\frac{\partial}{\partial X}\left(Pr\frac{\mu_{nf}}{\mu_f}\frac{\partial U}{\partial X}\right)+\frac{1}{\varepsilon}\frac{\partial}{\partial Y}\left(Pr\frac{\mu_{nf}}{\mu_f}\frac{\partial U}{\partial Y}\right)-\frac{Pr\mu_{eff}}{\mu_{nf}K^*(X,Y)Da}U\right)^n, \tag{17}$$

$$\frac{(V^*-V^n)}{\varepsilon}\frac{\rho_{nf}}{\rho_f} = \Delta\tau\left(\frac{1}{\varepsilon}\frac{\partial}{\partial X}\left(Pr\frac{\mu_{nf}}{\mu_f}\frac{\partial V}{\partial X}\right)+\frac{1}{\varepsilon}\frac{\partial}{\partial Y}\left(Pr\frac{\mu_{nf}}{\mu_f}\frac{\partial V}{\partial Y}\right)-\frac{Pr\mu_{eff}}{\mu_{nf}K^*(X,Y)Da}V+\frac{(\rho\beta)_{nf}}{(\rho\beta)_f}PrRa\theta\right)^n, \tag{18}$$

Solving PPE:

$$\nabla^2 P^{n+1} = \frac{\rho}{\Delta\tau}\left(\frac{\partial U^*}{\partial X}+\frac{\partial V^*}{\partial Y}\right)+\alpha\frac{\rho-\rho^{num}}{\Delta\tau^2}, \tag{19}$$

The final velocities are:

$$U^{n+1}-U^* = -\Delta\tau\left(\frac{1}{\rho}\nabla P^{n+1}\right), \tag{20}$$

$$V^{n+1}-V^* = -\Delta\tau\left(\frac{1}{\rho}\nabla P^{n+1}\right), \tag{21}$$

Thermal energy equation:

$$(\theta^{n+1}-\theta^n)\frac{(\rho c_p)_{nf}}{(\rho c_p)_f} = \Delta\tau\left[\frac{\partial}{\partial X}\left(\zeta(X,Y)\frac{\partial\theta}{\partial X}\right)+\frac{\partial}{\partial Y}\left(\zeta(X,Y)\frac{\partial\theta}{\partial Y}\right)\right]^n, \tag{22}$$

The positions are updated as:

$$X^{n+1} = \Delta\tau U^{n+1}+X^n, \tag{23}$$

$$Y^{n+1} = \Delta\tau V^{n+1}+Y^n. \tag{24}$$

The shifting technique:

$$\Upsilon_{i'} = (\nabla\Upsilon)_i\delta R_{ii'}+o(\delta R_{ii'}^2)+\Upsilon_i. \tag{25}$$

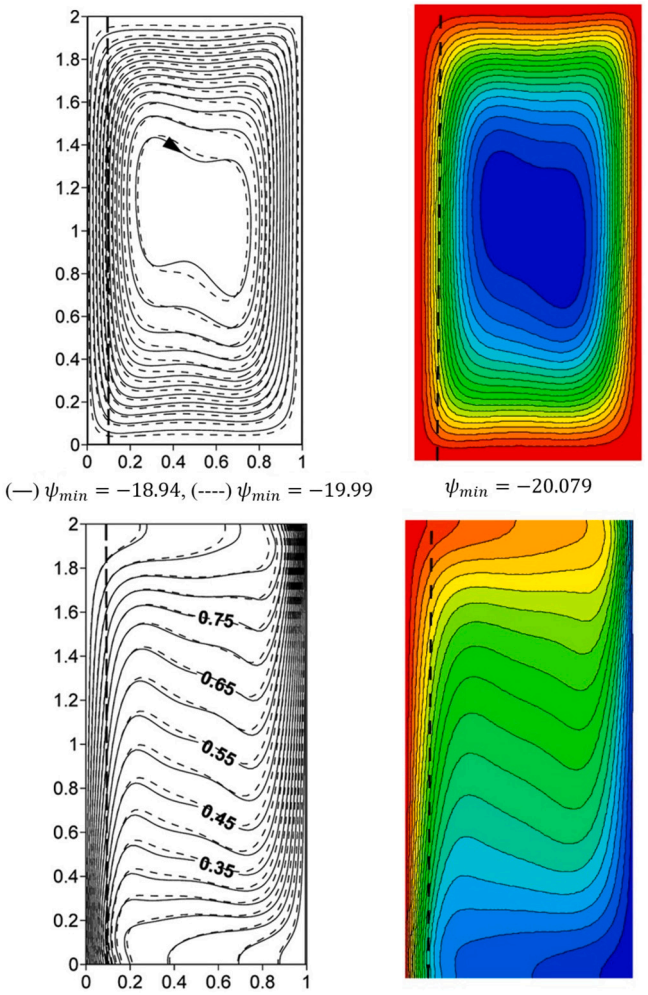

Fig. 3. The streamlines (top) and isotherms (bottom) from Chamkha and Ismael [46] (left) and the ISPH method (right) at $\phi = 5\%$, $Ra = 10^5$, $A = 2, X_p = 0.1$.

4. Validation tests

This section introduces two numerical tests to prove the efficiency of the used ISPH method in simulating fluid flows through porous media. Fig. 2 introduces the temperature profiles in a partial porous cavity from the ISPH method and experimental/numerical results of Beckermann et al. [45]. Here, the ISPH method showed a well agreement between the ISPH method and experimental/numerical results of Beckermann et al. [45] for natural convection in a partitioned porous cavity. Another validation test is introduced in Fig. 3. In this numerical test, the streamlines and isotherms for natural convection in a partitioned porous cavity at $\phi = 5\%$, $Ra = 10^5$, $A = 2, X_p = 0.1$ are compared between the ISPH method and Chamkha and Ismael [46]. This numerical test confirms the efficiency of the ISPH method as it represents a well accordance compared to the results of Chamkha and Ismael [46].

The third validation test examines the natural convection from an inner hot rectangle inside a square cavity. Fig. 4 (a,b) represents the validation test between the ISPH method and numerical/experimental data of Paroncini and Corvaro [47]. Here, the streamlines and isotherms across a cavity at Hot rectangle length = 0.5 with (a) $Ra = 1.78x10^5$ and (b) $Ra = 2.25x10^5$ are obtained. It is found that the streamlines and isotherms agree well between the ISPH method and Paroncini and Corvaro [47]. From now, there is a confidence in the ISPH method for natural convection in a porous closed domain. Table 2 presents the comparison of $\overline{Nu}$ between the ISPH method and benchmark results from de Vahl Davis [48]. This validation shows the efficiency of the ISPH tool in calculating the $\overline{Nu}$ across the hot walls during natural convection flows.

5. Results and discussions

This section presents the obtained simulations for time-dependent natural convection flow of a nanofluid inside a circular cylinder cavity saturated with a porous medium. The simulations are carried out for several key factors including different types of the embedded structures, different thermal condition of structures, nanoparticles parameter $0 \le \phi \le 0.5$, porous medium level, and Darcy parameter $10^{-3} \le Da \le 10^{-5}$ on the fluid flow and characteristic heat transfer. Tracking the circular rotations of the embedded

Table 2
The value of $\overline{Nu}$ of the ISPH method and benchmark results [48].

Results of $\overline{Nu}$	$Ra = 10^3$	$Ra = 10^4$	$Ra = 10^5$
The ISPH method	0.988	2.154	4.141
de Vahl Davis [48]	1.116	2.234	4.487

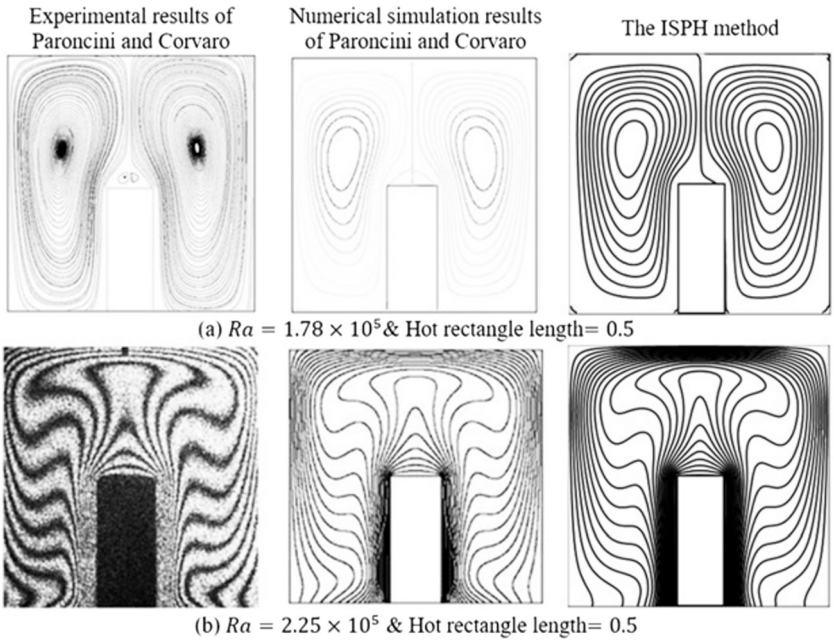

Fig. 4. The validation test between the ISPH method and numerical/experimental data of Paroncini and Corvaro [47].

structures was introduced. Fig. 5 (a-c) shows the circular motions of three embedded structures inside a cavity. In general, one of the advantages of the ISPH method are treating the coupling between fluid-structure interaction during natural convection flow by an easy way without a special treatment. In this figure, as the times increase from $\tau = 0.005$ sec to $\tau = 0.5$ sec, then the inner structure rotates circularly around the cavity's center.

Fig. 6 (a-c) represents the temperature distributions under the variations of heated/cooled area of embedded cylinder for (a) a homogeneous porous level, and (b) a heterogeneous porous level. It is seen that the temperature distributions inside the circular cavity are depending on the type, and positions of the inner structure. Due to the longest height between the triangle shape and outer domain, high temperature distributions were obtained at the case of inner triangle structure. So, it is well mentioned that a choosing of an inner structure plays a significant role in enhancement heat transfer within a closed domain. Fig. 7 (a,b) introduces the temperature distributions under the alterations of heated/cooled area of embedded circular cylinder for (a) a homogeneous porous level, and (b) a heterogeneous porous level. The temperature distributions are enhanced inside a circular cavity at the case of heated area of the inner cylinder, while as an increase on the cool area accompanied by a decrease on the heated area of inner cylinder are reducing the temperature distributions. Fig. 8 (a,b) represents the velocity fields under alterations of heated/cooled area of embedded cylinder inside a circular cylinder cavity for (a) a homogeneous porous level, and (b) a heterogeneous porous level. From this figure, as the circular cylinder rotates in a circular form, then the center of a circular cylinder has almost zero velocity. It is seen that, the maximum values of the velocity fields are given at the case of half hot/cold circular cylinder for both levels of homogeneous/heterogeneous porous media. Moreover, the maximum velocity increases as the level of the porous media changes from the homogeneous to heterogeneous porous level and the reason returns to the definition of K^* in equation (5) within the momentum equations (2)-(3). Figs. 9 (a,b)-10 (a,b) show the temperature and velocity distributions under the variations on the heated/cooled area of an embedded rectangle inside a circular cylinder cavity for (a) homogeneous porous level, and (b) heterogeneous porous level. Here, the whole hot rectangle augments the temperature distributions and it reduces the velocity fields inside a circular cylinder cavity. Physically, the inner shape represents as a blockage for the nanofluid flow and consequently it reduces the strength of the velocity fields within a cavity. It is seen that, there are slight changes on the temperature distributions under the variations of the level of porous media. The homogeneous porous level reduces the velocity fields compare to the heterogeneous porous level. Figs. 11 (a,b)-12 (a,b) show the temperature distributions under the variations of the heated/cooled area of embedded triangle inside a circular cylinder cavity for (a) homogeneous porous level, and (b) heterogeneous porous level. In this figure, the whole

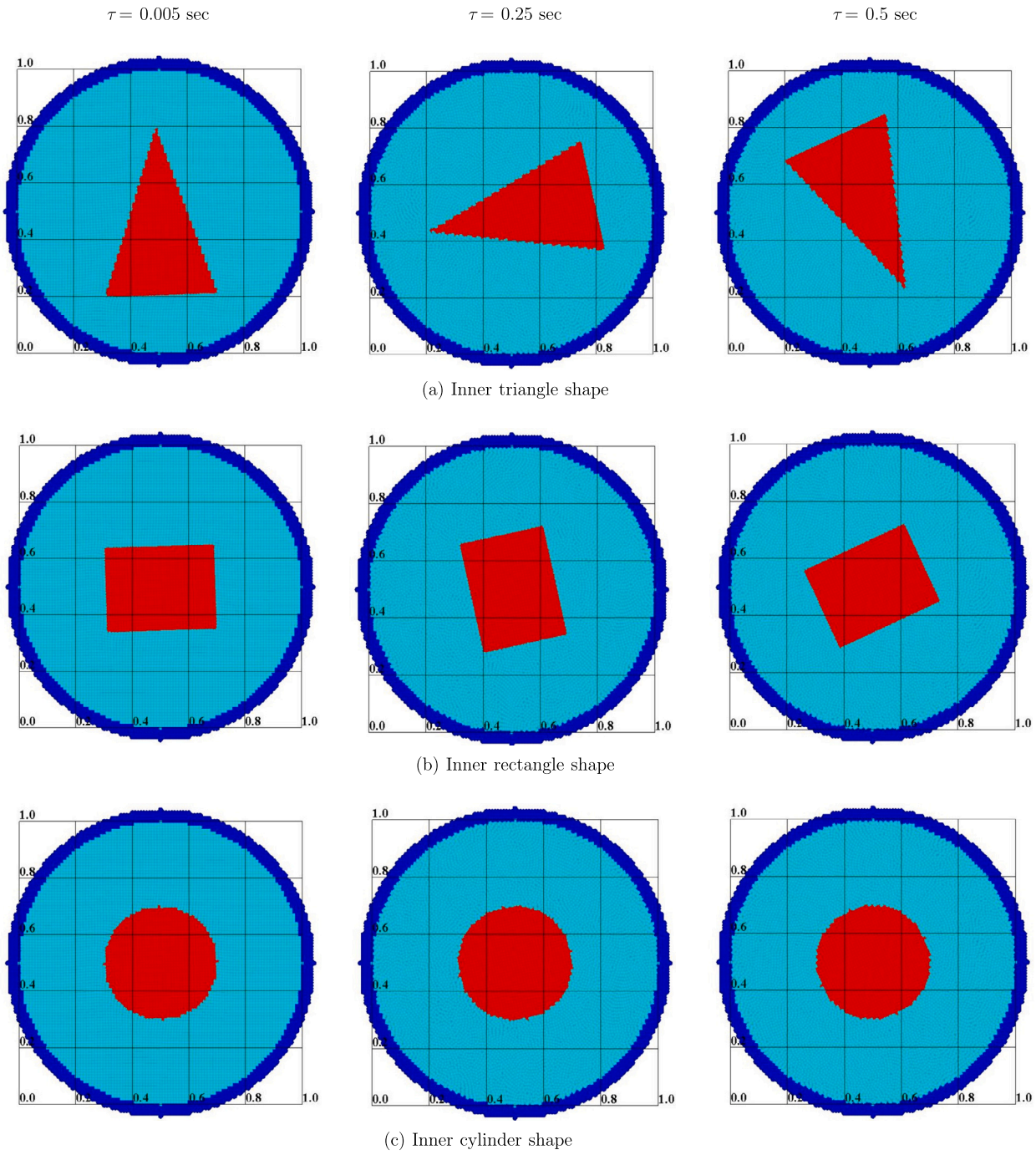

Fig. 5. Time histories of the circular motions of the three embedded structures inside a circular cylinder cavity at the case of half heated part of an inner shape, a homogeneous porous level, $R = 0.5$, $Ra = 10^4$, $\phi = 0.01$, $Da = 10^{-3}$ and $\varepsilon = 0.6$.

triangle raises the temperature distributions and reduces the velocity fields at the case of homogeneous porous medium level. The heterogeneous porous level augments the maximum of the velocity field inside a circular cylinder cavity.

Figs. 13-14 depict the impacts of the temperature distributions and velocity fields inside a circular cylinder cavity under the impacts of nanoparticles parameter ϕ at half hot/cold rectangle, and heterogeneous porous level. Adding nanoparticles concentration enhances the temperature distributions in a circular cylinder cavity. Physically, adding extra concentration of nanoparticles increases the viscosity of the base fluid and consequently the velocity fields are reducing inside a circular cylinder cavity. Figs. 15 (a,b)-16 (a,b) present the temperature distributions and velocity fields inside a circular cylinder cavity under the impacts of Darcy parameter for half hot/cold rectangle at two cases of (a) homogeneous porous level, and (b) heterogeneous porous level. It is found that the Darcy

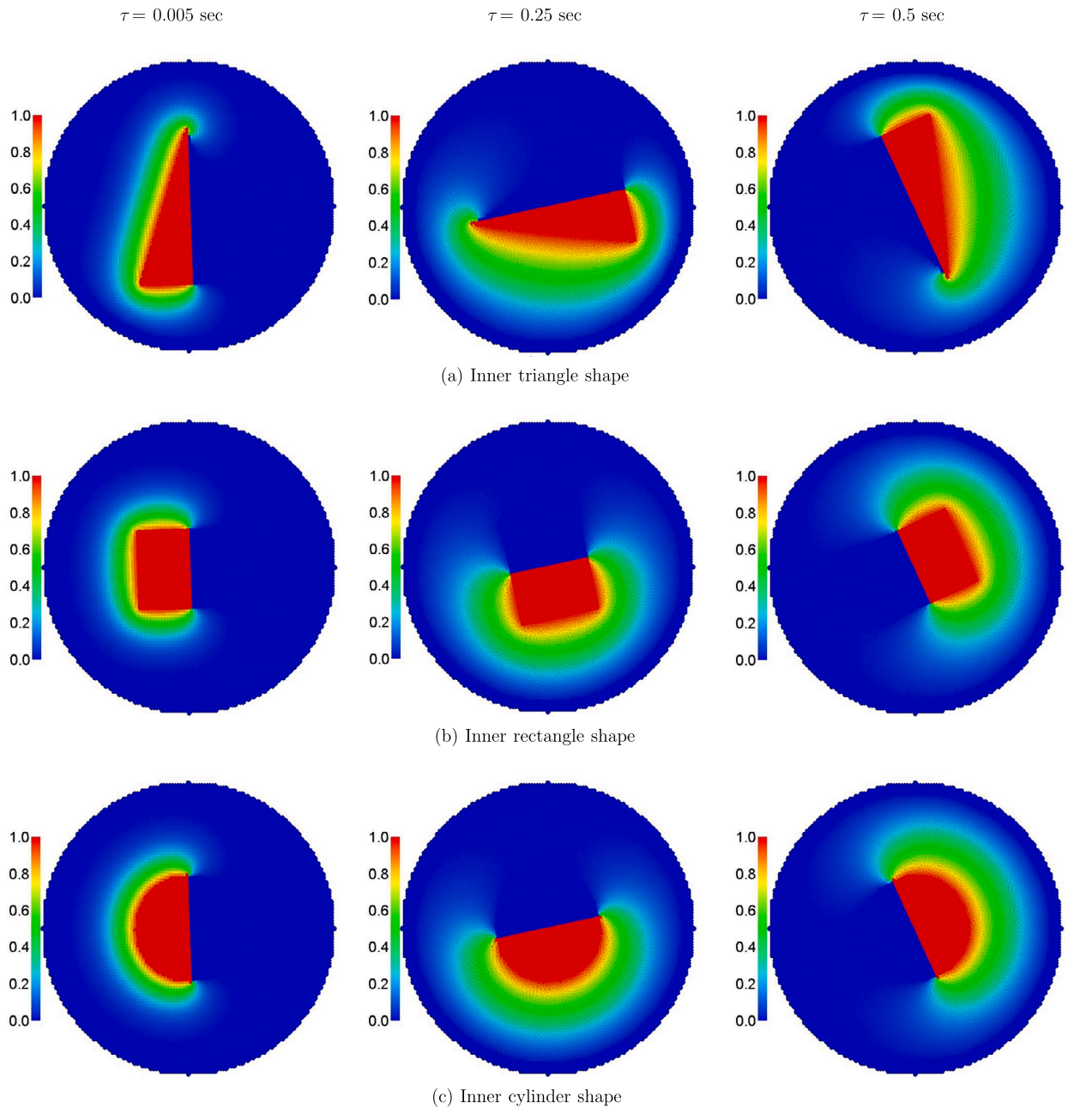

Fig. 6. Time histories of the temperature distributions of the three embedded shapes inside a circular cylinder cavity at the case of half heated part of an inner shape, a homogeneous porous level, $R = 0.5$, $Ra = 10^4$, $\phi = 0.01$, $Da = 10^{-3}$ and $\varepsilon = 0.6$.

parameter has slight effects on the temperature distributions inside a cavity and as Da decreases from $Da = 10^{-3}$ to $Da = 10^{-5}$, the velocity fields around the inner cylinder are decreasing. It is seen that, the maximum of the velocity field increases from 3 at the case of $Da = 10^{-3}$ with a homogeneous porous level to 3.9 at the case of $Da = 10^{-3}$ with a heterogeneous porous level, while at $Da \geq 10^{-4}$, there are no variations on the maximum values of the velocity fields between the homogeneous and heterogeneous porous level. Due to the circular rotation of the inner circular cylinder, the maximum values of the velocity fields are occurring only at the area between the fluid flow and inner circular cylinder. The physical reason of these results return to the high porous resistance at a lower Darcy parameter.

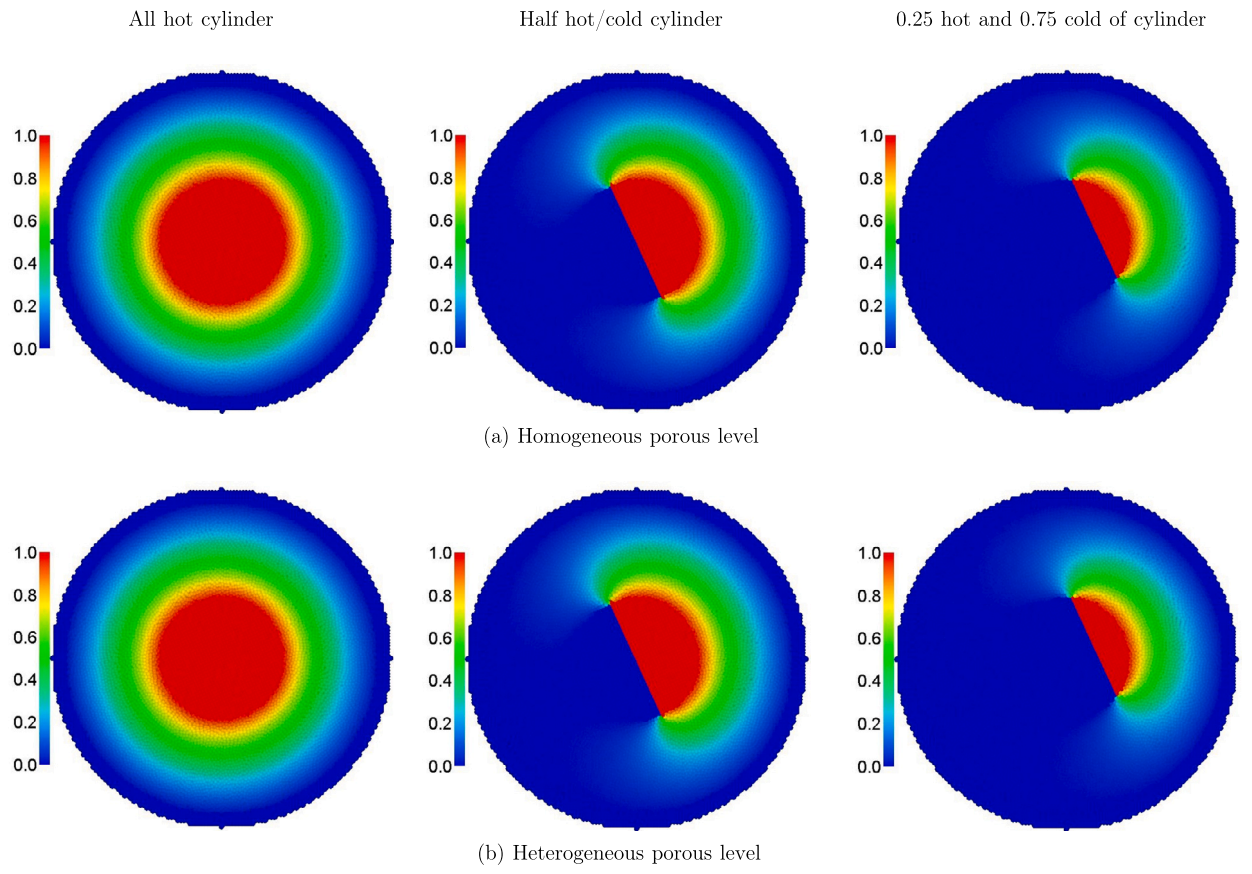

Fig. 7. Temperature distributions under the variations on the heated/cooled area of embedded cylinder inside a circular cylinder cavity for (a) Homogeneous porous level, (b) Heterogeneous porous level at $R = 0.5$, $Ra = 10^4$, $\phi = 0.01$, $Da = 10^{-3}$ and $\varepsilon = 0.6$.

6. Conclusion

Natural convection of Al_2O_3 - H_2O in a circular cylinder cavity saturated by a heterogeneous/homogeneous porous media was numerically simulated in the presence of three different inner structures having a circular rotation. The novelty of this work is appeared in adopting the ISPH method for simulating convection flow of circular rotation of different solid structures in a closed circular cylinder. It was observed that the maximum values of the velocity field are occurring between the embedded structure and the surrounding nanofluids. The installation of the inner hot/cold structures changes the temperature distributions and nanofluid flows inside a circular cylinder cavity. The inner triangle structure has the biggest effect on the temperature distributions and velocity fields due to its longest height inside a cylinder domain. The rotation of the embedded structures changes the temperature distributions and velocity field within a circular cylinder. Hence, the current problem can be applied in enhancement the heat transfer performance in solar collectors and designing energy devices with inner structures. The variations of hot/cold parts of the embedded structure have strong impacts on the temperature and velocity fields inside the circular cylinder. Even if the whole heated structure gives the high temperature distribution inside a cavity, but it has a lowest maximum value of the velocity field due to large blockage. The homogeneous porous level is reducing the maximum values of the velocity fields by 25% compare to the heterogeneous porous level.

CRediT authorship contribution statement

Abdelraheem M. Aly: Conceived and designed the experiments; Performed the experiments; Contributed reagents, materials, analysis tools or data.

Zehba Raizah: Performed the experiments; Analyzed and interpreted the data; Wrote the paper.

Ali J. Chamkha Analyzed and interpreted the data; Contributed reagents, materials, analysis tools or data; Wrote the paper.

Declaration of competing interest

The authors declare that they have NO affiliations with or involvement in any organization or entity with any financial interest.

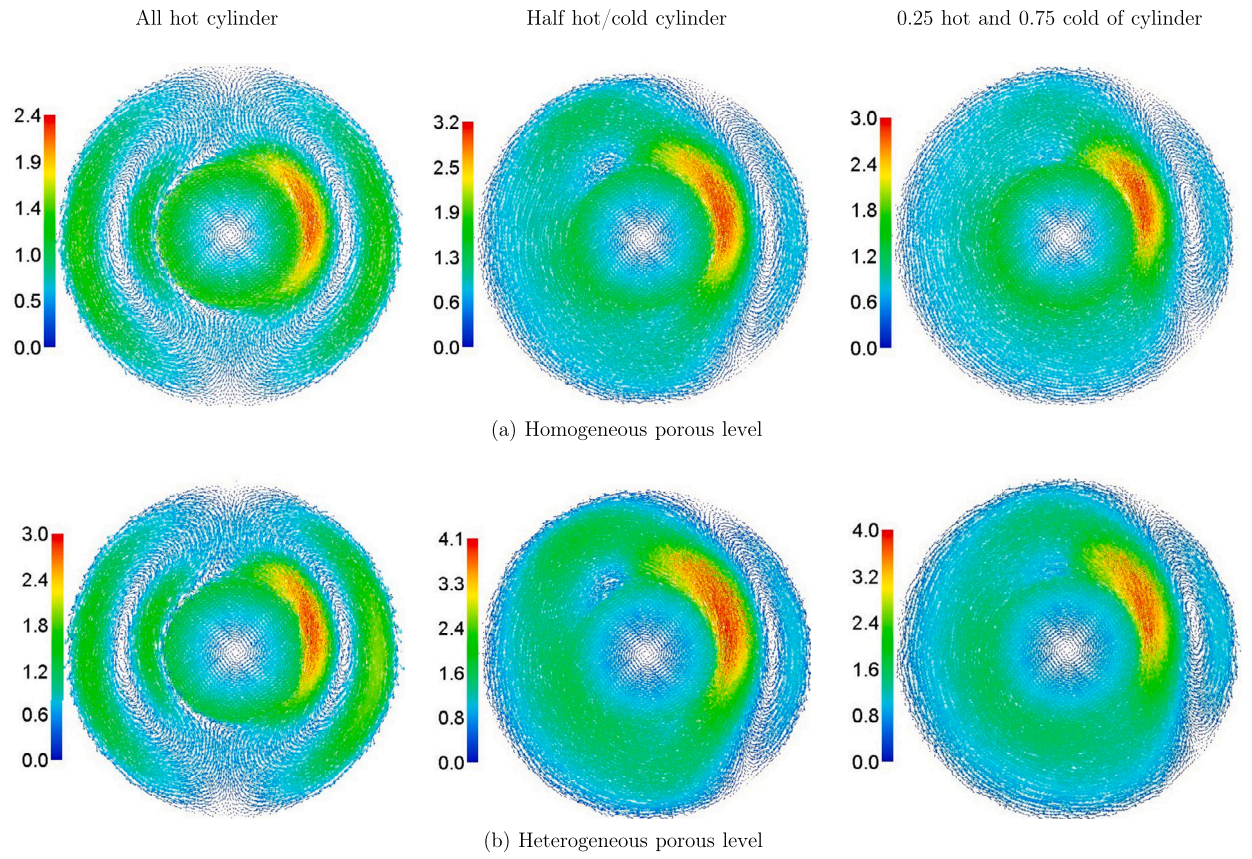

Fig. 8. Velocity fields under the variations on the heated/cooled area of embedded cylinder inside a circular cylinder cavity for (a) Homogeneous porous level, (b) Heterogeneous porous level at $R = 0.5$, $Ra = 10^4$, $\phi = 0.01$, $Da = 10^{-3}$ and $\epsilon = 0.6$.

Acknowledgements

The authors extend their appreciation to the Deanship of Scientific Research at King Khalid University, Abha, Saudi Arabia, for funding this work through the research group project under grant number (RGP. 1/505/44).

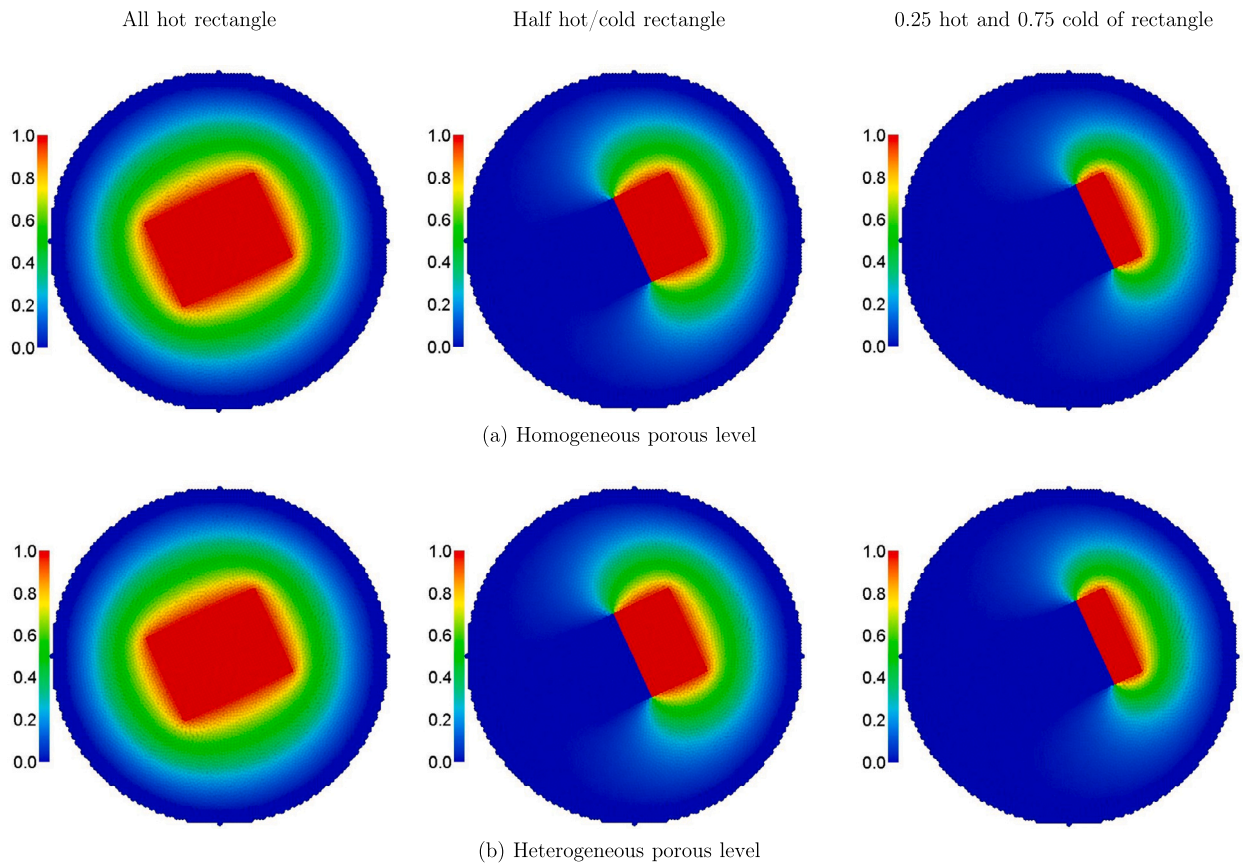

Fig. 9. Temperature distributions under the variations on the heated/cooled area of embedded rectangle inside a circular cylinder cavity for (a) Homogeneous porous level, (b)Heterogeneous porous level at $R = 0.5$, $Ra = 10^4$, $\phi = 0.01$, $Da = 10^{-3}$ and $\varepsilon = 0.6$.

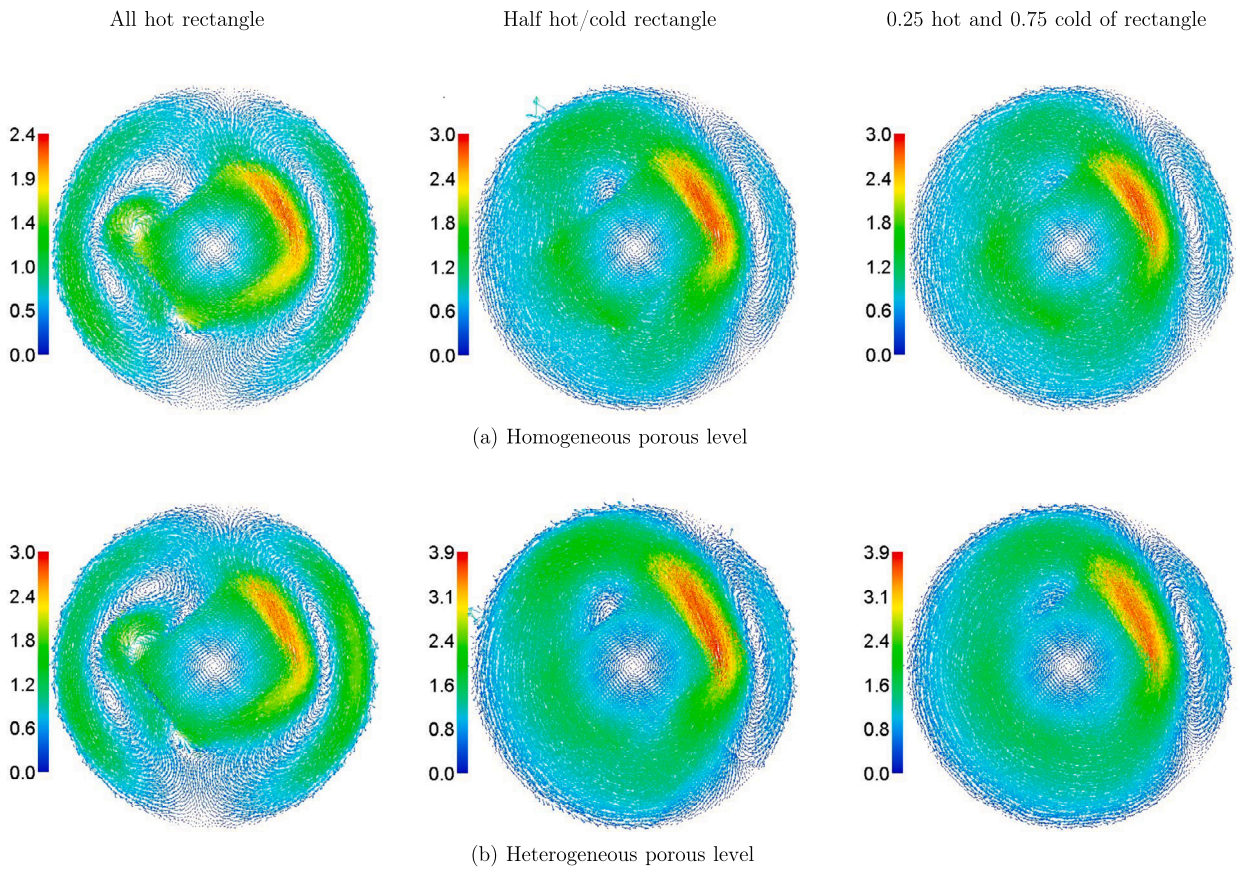

Fig. 10. Velocity fields under the variations on the heated/cooled area of embedded rectangle inside a circular cylinder cavity for (a) Homogeneous porous level, (b) Heterogeneous porous level at $R = 0.5$, $Ra = 10^4$, $\phi = 0.01$, $Da = 10^{-3}$ and $\varepsilon = 0.6$.

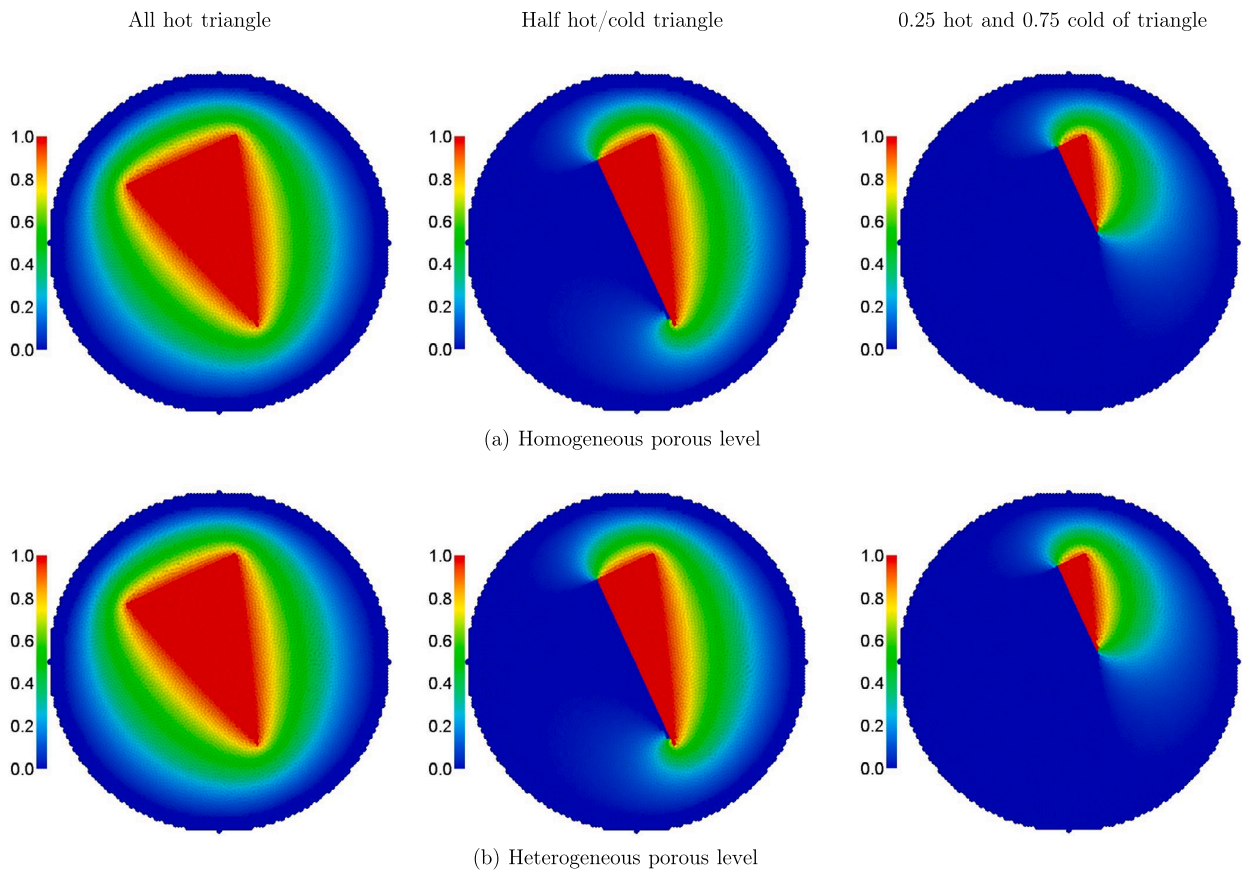

Fig. 11. Temperature distributions under the variations on the heated/cooled area of embedded triangle inside a circular cylinder cavity for (a) Homogeneous porous level, (b) Heterogeneous porous level at $R = 0.5$, $Ra = 10^4$, $\phi = 0.01$, $Da = 10^{-3}$ and $\varepsilon = 0.6$.

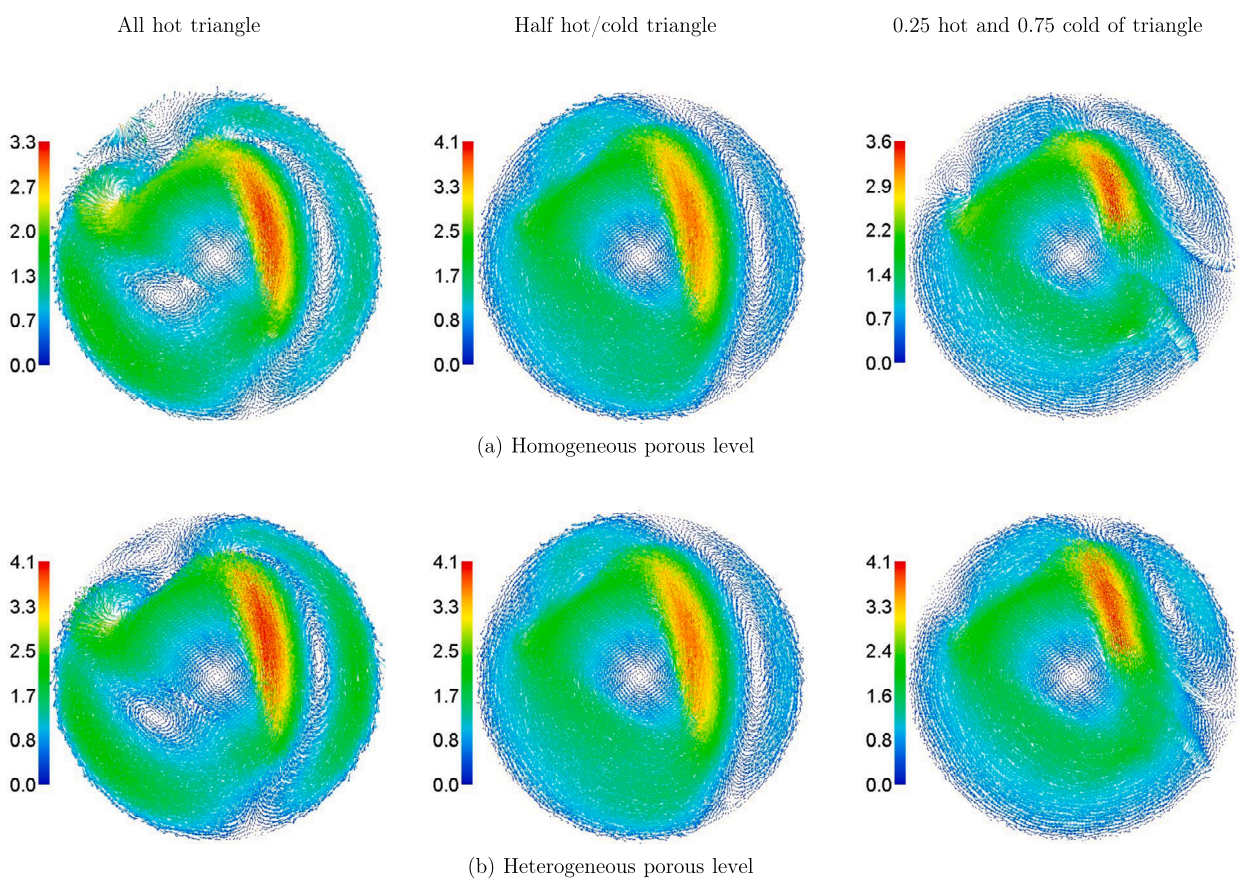

Fig. 12. Velocity fields under the variations on the heated/cooled area of embedded triangle inside a circular cylinder cavity for (a) Homogeneous porous level, (b) Heterogeneous porous level at $R = 0.5$, $Ra = 10^4$, $\phi = 0.01$, $Da = 10^{-3}$ and $\varepsilon = 0.6$.

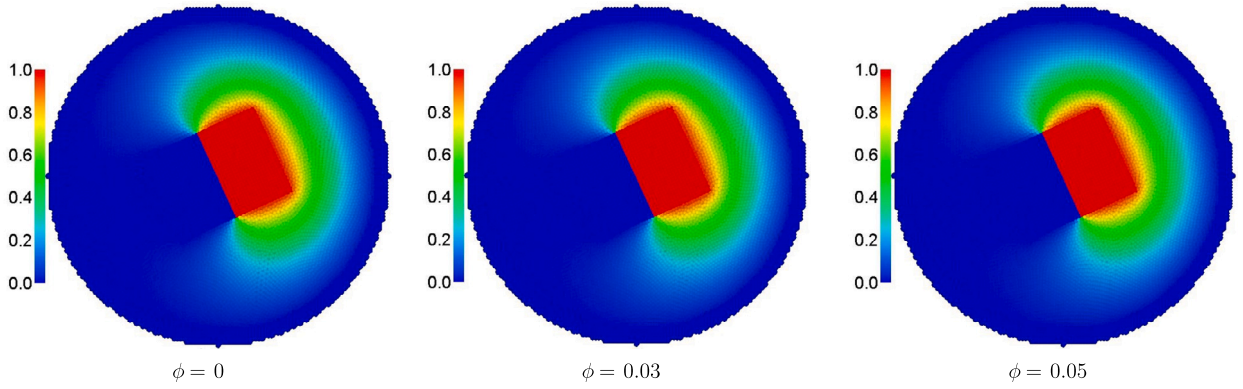

Fig. 13. Temperature distributions inside a circular cylinder cavity under the impacts of nanoparticles parameter ϕ at half hot/cold rectangle, Heterogeneous porous level, $R = 0.5$, $Ra = 10^4$, $Da = 10^{-4}$ and $\varepsilon = 0.6$.

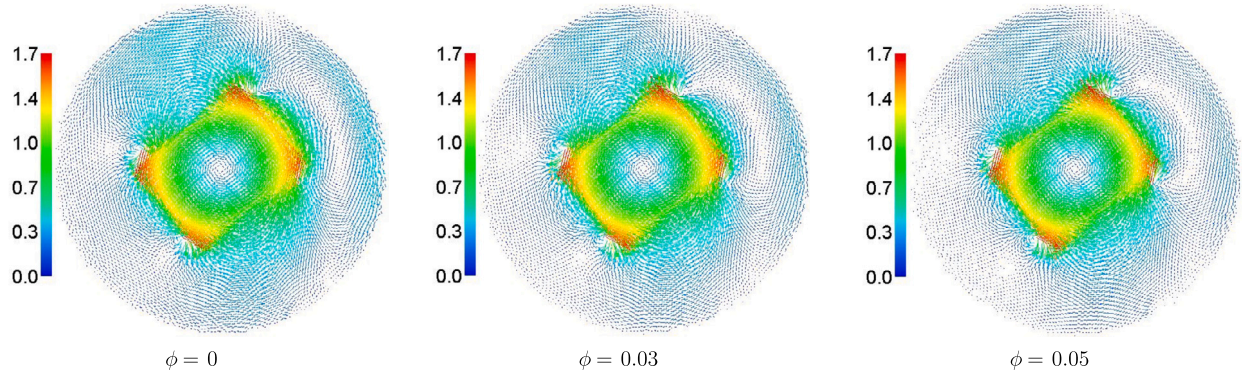

Fig. 14. Velocity fields inside a circular cylinder cavity under the impacts of nanoparticles parameter ϕ at half hot/cold rectangle, Heterogeneous porous level, $R = 0.5$, $Ra = 10^4$, $Da = 10^{-4}$ and $\varepsilon = 0.6$.

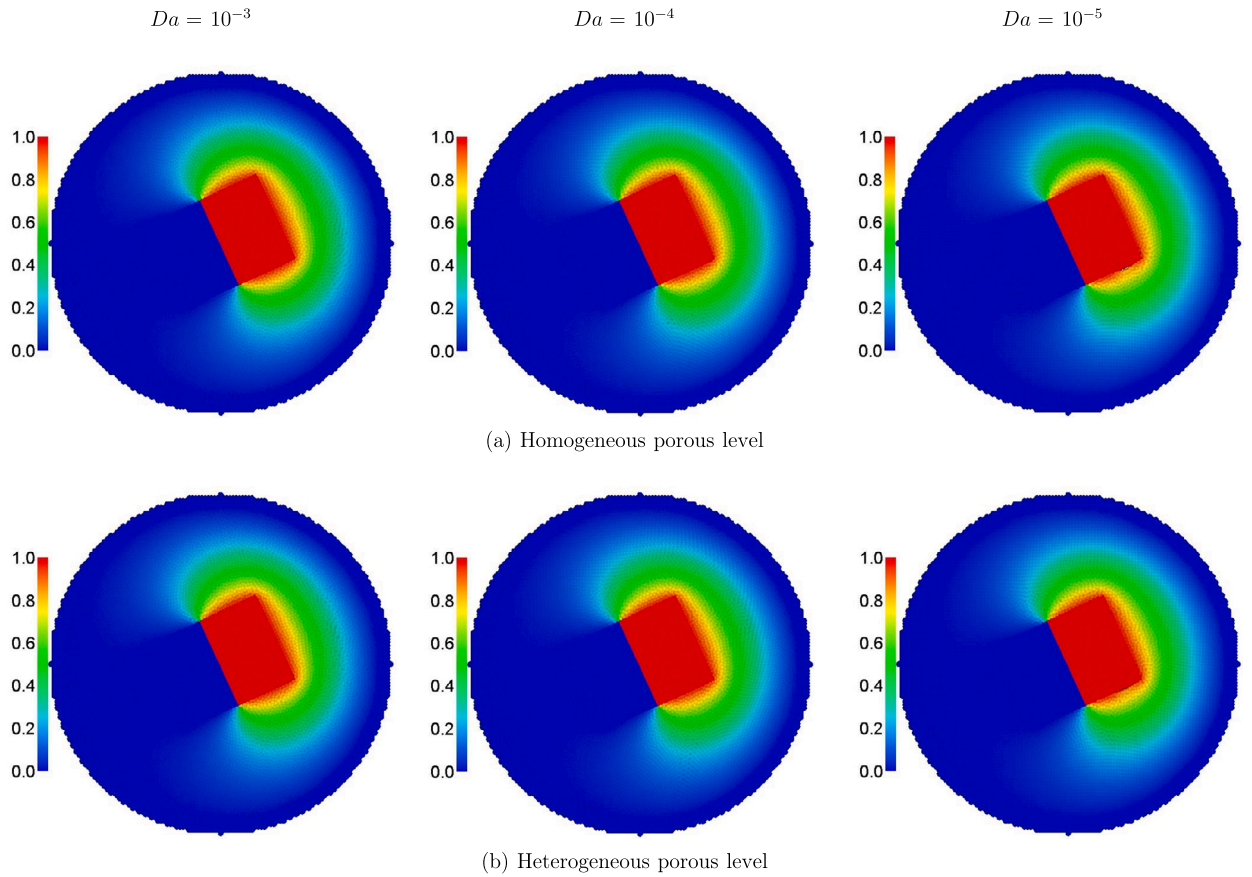

Fig. 15. Temperature distributions inside a circular cylinder cavity under the impacts of Darcy parameter for half hot/cold rectangle at two cases of (a) Homogeneous porous level, (b) Heterogeneous porous level, $R = 0.5$, $Ra = 10^4$, $\phi = 0.01$, $Da = 10^{-3}$ and $\varepsilon = 0.6$.

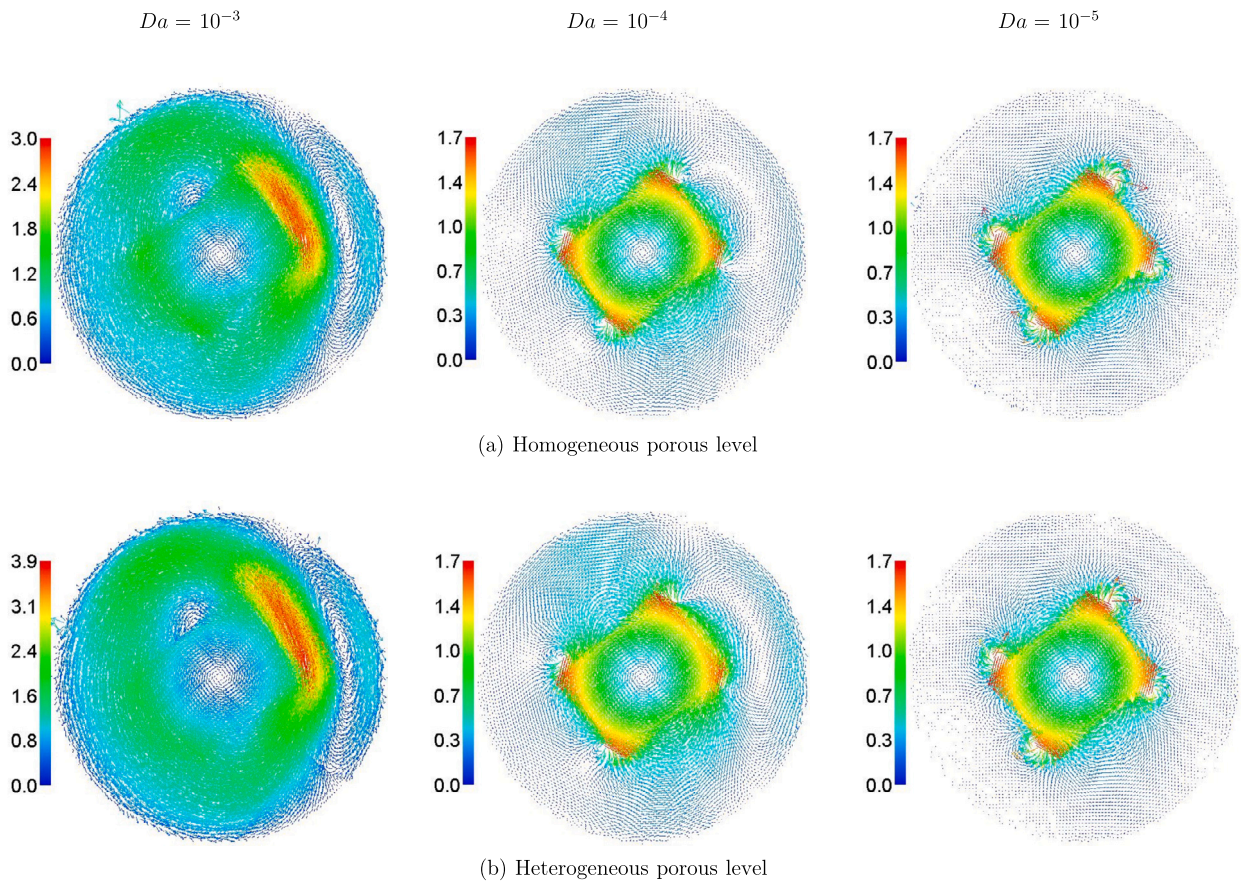

Fig. 16. Velocity fields inside a circular cylinder cavity under the impacts of Darcy parameter for half hot/cold rectangle at two cases of (a) Homogeneous porous level, (b) Heterogeneous porous level, $R = 0.5$, $Ra = 10^4$, $\phi = 0.01$, $Da = 10^{-3}$ and $\epsilon = 0.6$.

References

[1] T. Hayase, J.A.C. Humphrey, R. Greif, Numerical calculation of convective heat transfer between rotating coaxial cylinders with periodically embedded cavities, J. Heat Transf. 114 (3) (08 1992) 589–597.
[2] Wu-Shung Fu, Chao-Sheng Cheng, Wen-Jiann Shieh, Enhancement of natural convection heat transfer of an enclosure by a rotating circular cylinder, Int. J. Heat Mass Transf. 37 (13) (1994) 1885–1897.
[3] Hakan F. Oztop, Zepu Zhao, Bo Yu, Fluid flow due to combined convection in lid-driven enclosure having a circular body, Int. J. Heat Fluid Flow 30 (5) (2009) 886–901, The 3rd International Conference on Heat Transfer and Fluid Flow in Microscale.
[4] Sachin B. Paramane, Atul Sharma, Numerical investigation of heat and fluid flow across a rotating circular cylinder maintained at constant temperature in 2-d laminar flow regime, Int. J. Heat Mass Transf. 52 (13) (2009) 3205–3216.
[5] Fatih Selimefendigil, Muneer A. Ismael, Ali J. Chamkha, Mixed convection in superposed nanofluid and porous layers in square enclosure with inner rotating cylinder, Int. J. Mech. Sci. 124–125 (2017) 95–108.
[6] Aydin Misirlioglu, The effect of rotating cylinder on the heat transfer in a square cavity filled with porous medium, Int. J. Eng. Sci. 44 (18) (2006) 1173–1187.
[7] Hyun Sik Yoon, Jeong Hu Kim, Ho Hwan Chun, Hee Jong Choi, Laminar flow past two rotating circular cylinders in a side-by-side arrangement, Phys. Fluids 19 (12) (2007) 128103.
[8] V.A.F. Costa, A.M. Raimundo, Steady mixed convection in a differentially heated square enclosure with an active rotating circular cylinder, Int. J. Heat Mass Transf. 53 (5) (2010) 1208–1219.
[9] Fatih Selimefendigil, Hakan F. Öztop, Mhd mixed convection of nanofluid filled partially heated triangular enclosure with a rotating adiabatic cylinder, J. Taiwan Inst. Chem. Eng. 45 (5) (2014) 2150–2162.
[10] R. Roslan, H. Saleh, I. Hashim, Effect of rotating cylinder on heat transfer in a square enclosure filled with nanofluids, Int. J. Heat Mass Transf. 55 (23) (2012) 7247–7256.
[11] Fatih Selimefendigil, Hakan F. Öztop, Mhd mixed convection and entropy generation of power law fluids in a cavity with a partial heater under the effect of a rotating cylinder, Int. J. Heat Mass Transf. 98 (2016) 40–51.
[12] Salam Hadi Hussain, Ahmed Kadhim Hussein, Mixed convection heat transfer in a differentially heated square enclosure with a conductive rotating circular cylinder at different vertical locations, Int. Commun. Heat Mass Transf. 38 (2) (2011) 263–274.
[13] Ali Khaleel Kareem, Shian Gao, Mixed convection heat transfer of turbulent flow in a three-dimensional lid-driven cavity with a rotating cylinder, Int. J. Heat Mass Transf. 112 (2017) 185–200.
[14] Ammar I. Alsabery, Tahar Tayebi, Ali J. Chamkha, Ishak Hashim, Effect of rotating solid cylinder on entropy generation and convective heat transfer in a wavy porous cavity heated from below, Int. Commun. Heat Mass Transf. 95 (2018) 197–209.
[15] Xiaoke Ku, Heng Li, Jianzhong Lin, Hanhui Jin, Accumulation of heavy particles in circular bounded vortex flows induced by two small rotating cylinders, Int. J. Multiph. Flow 113 (2019) 71–88.

[16] Abdelraheem M. Aly, Natural convection over circular cylinders in a porous enclosure filled with a nanofluid under thermo-diffusion effects, J. Taiwan Inst. Chem. Eng. 70 (2017) 88–103.
[17] Lioua Kolsi, Fatih Selimefendigil, Hatem Gasmi, Badr M. Alshammari, Conjugate heat transfer analysis for cooling of a conductive panel by combined utilization of nanoimpinging jets and double rotating cylinders, Nanomaterials 13 (3) (2023).
[18] Hana Ouri, Fatih Selimefendigil, Mourad Bouterra, Mohamed Omri, Badr M. Alshammari, Lioua Kolsi, Mhd hybrid nanofluid convection and phase change process in an l-shaped vented cavity equipped with an inner rotating cylinder and pcm-packed bed system, Alex. Eng. J. 63 (2023) 563–582.
[19] Fatih Selimefendigil, Mondher Hamzaoui, Abdelkarim Aydi, Badr M. Alshammari, Lioua Kolsi, Hybrid nano-jet impingement cooling of double rotating cylinders immersed in porous medium, Mathematics 11 (1) (2023).
[20] Wael Al-Kouz, Abderrahmane Aissa, S. Suriya Uma Devi, M. Prakash, Lioua Kolsi, Hazim Moria, Wasim Jamshed, Obai Younis, Effect of a rotating cylinder on the 3d mhd mixed convection in a phase change material filled cubic enclosure, Sustain. Energy Technol. Assess. 51 (2022) 101879.
[21] K. Christou, W.C. Radünz, B. Lashore, F.B.S. de Oliveira, J.L.M.A. Gomes, Numerical investigation of viscous flow instabilities in multiphase heterogeneous porous media, Adv. Water Resour. 130 (2019) 46–65.
[22] Y.J. Zhuang, Q.Y. Zhu, Analysis of entropy generation in combined buoyancy-marangoni convection of power-law nanofluids in 3d heterogeneous porous media, Int. J. Heat Mass Transf. 118 (2018) 686–707.
[23] Boyu He, Shihua Lu, Dongyan Gao, Weiwei Chen, Fujian Lin, Lattice boltzmann simulation of double diffusive natural convection in heterogeneously porous media of a fluid with temperature-dependent viscosity, Chin. J. Phys. 63 (2020) 186–200.
[24] Chunyan Liu, Mingyang Pan, Liancun Zheng, Ping Lin, Effects of heterogeneous catalysis in porous media on nanofluid-based reactions, Int. Commun. Heat Mass Transf. 110 (2020) 104434.
[25] Mohamad Chaaban, Yousef Heider, Bernd Markert, Upscaling lbm-tpm simulation approach of darcy and non-darcy fluid flow in deformable, heterogeneous porous media, Int. J. Heat Fluid Flow 83 (2020) 108566.
[26] I. Federico, S. Marrone, A. Colagrossi, F. Aristodemo, M. Antuono, Simulating 2d open-channel flows through an sph model, Eur. J. Mech. B, Fluids 34 (2012) 35–46.
[27] Abbas Khayyer, Hitoshi Gotoh, Songdong Shao, Enhanced predictions of wave impact pressure by improved incompressible sph methods, Appl. Ocean Res. 31 (2) (2009) 111–131.
[28] Abdelraheem M. Aly, Sang-Wook Lee, Numerical simulations of impact flows with incompressible smoothed particle hydrodynamics, J. Mech. Sci. Technol. 28 (6) (2014) 2179–2188.
[29] Hitoshi Gotoh, Abbas Khayyer, Hiroyuki Ikari, Taro Arikawa, Kenichiro Shimosako, On enhancement of incompressible sph method for simulation of violent sloshing flows, Appl. Ocean Res. 46 (2014) 104–115.
[30] Abdelraheem M. Aly, Mitsuteru Asai, Ali J. Chamkha, Analysis of unsteady mixed convection in lid-driven cavity included circular cylinders motion using an incompressible smoothed particle hydrodynamics method, Int. J. Numer. Methods Heat Fluid Flow (2015).
[31] Abdelraheem M. Aly, Double-diffusive natural convection in an enclosure including/excluding sloshing rod using a stabilized isph method, Int. Commun. Heat Mass Transf. 73 (2016) 84–99.
[32] Abdelraheem M. Aly, Z.A.S. Raizah, Incompressible smoothed particle hydrodynamics (isph) method for natural convection in a nanofluid-filled cavity including rotating solid structures, Int. J. Mech. Sci. 146–147 (2018) 125–140.
[33] Abdelraheem M. Aly, Mitsuteru Asai, Modelling of non-darcy flows through porous media using extended incompressible smoothed particle hydrodynamics, Numer. Heat Transf., Part B, Fundam. 67 (3) (2015) 255–279.
[34] Abdelraheem M. Aly, Sameh E. Ahmed, An incompressible smoothed particle hydrodynamics method for natural/mixed convection in a non-darcy anisotropic porous medium, Int. J. Heat Mass Transf. 77 (2014) 1155–1168.
[35] Abdelraheem M. Aly, Mitsuteru Asai, Three-dimensional incompressible smoothed particle hydrodynamics for simulating fluid flows through porous structures, Transp. Porous Media 110 (3) (2015) 483–502.
[36] Minh Tuan Nguyen, Abdelraheem M. Aly, Sang-Wook Lee, A numerical study on unsteady natural/mixed convection in a cavity with fixed and moving rigid bodies using the isph method, Int. J. Numer. Methods Heat Fluid Flow (2018).
[37] F. Awad, Z.A.S. Raizah, Abdelraheem M. Aly, ISPH simulation of impact flow of circular cylinder over free surface porous media, J. Braz. Soc. Mech. Sci. Eng. 45 (2023) 324–335.
[38] Abdelraheem M. Aly, Zehba AS Raizah, Coupled fluid-structure interactions of natural convection in a ferrofluid using isph method, Alex. Eng. J. 58 (4) (2019) 1499–1516.
[39] Abdelraheem M. Aly, Natural convection of a nanofluid-filled circular enclosure partially saturated with a porous medium using isph method, Int. J. Numer. Methods Heat Fluid Flow (2020).
[40] Zehba A.S. Raizah, Sameh E. Ahmed, Abdelraheem M. Aly, Isph simulations of natural convection flow in e-enclosure filled with a nanofluid including homogeneous/heterogeneous porous media and solid particles, Int. J. Heat Mass Transf. 160 (2020) 120153.
[41] Abdelraheem M. Aly, Zehba Raizah, Hijaz Ahmed, Amal M. Al-Hanaya, Noura Alsedias, Double diffusion in a combined cavity occupied by a nanofluid and heterogeneous porous media, Open Phys. 20 (1) (2022) 891–904.
[42] Zehba A.S. Raizah, Abdelraheem M. Aly, Sameh E. Ahmed, Natural convection flow of a nanofluid-filled v-shaped cavity saturated with a heterogeneous porous medium: incompressible smoothed particle hydrodynamics analysis, Ain Shams Eng. J. 12 (2) (2021) 2033–2046.
[43] Y.J. Zhuang, Q.Y. Zhu, Numerical study on combined buoyancy–marangoni convection heat and mass transfer of power-law nanofluids in a cubic cavity filled with a heterogeneous porous medium, Int. J. Heat Fluid Flow 71 (2018) 39–54.
[44] Massimo Corcione, Empirical correlating equations for predicting the effective thermal conductivity and dynamic viscosity of nanofluids, Energy Convers. Manag. 52 (1) (2011) 789–793.
[45] C. Beckermann, S. Ramadhyani, R. Viskanta, Natural convection flow and heat transfer between a fluid layer and a porous layer inside a rectangular enclosure, J. Heat Transf. 109 (2) (05 1987) 363–370.
[46] Ali J. Chamkha, Muneer A. Ismael, Natural convection in differentially heated partially porous layered cavities filled with a nanofluid, Numer. Heat Transf., Part A, Appl. 65 (11) (2014) 1089–1113.
[47] M. Paroncini, F. Corvaro, Natural convection in a square enclosure with a hot source, Int. J. Therm. Sci. 48 (9) (2009) 1683–1695.
[48] G. De Vahl Davis, Natural convection of air in a square cavity: a bench mark numerical solution, Int. J. Numer. Methods Fluids 3 (3) (1983) 249–264.